iSplash: Realizing Fast Carangiform Swimming to Outperform a Real Fish

Richard James Clapham and Huosheng Hu

Abstract This paper focuses on the linear swimming motion of Carangiform fish and presents two novel prototypes: *iSplash*-I and *iSplash*-II, which have overcome some of the previously known challenges, in particular the straight line swimming speed of robotic fish. The first generation *iSplash*-I improved the kinematic pattern by deploying a full-body length swimming motion to coordinate anterior, mid-body, and posterior displacements. The second generation *iSplash*-II achieved consistent untethered stabilized swimming speeds of 11.6 BL/s (i.e., 3.7 m/s), with a frequency of 20 Hz during the field trials, outperforming real carangiform fish in terms of average maximum velocity (measured in body lengths/second) and endurance, the duration that top speed is maintained.

Keywords Robotic fish · Carangiform swimming · Full-Body length · Swimming speed · Maximum velocity

1 Introduction

To navigate through a marine environment, a robotic vehicle requires mobility to effectively contend with the physical forces exerted by the surrounding fluid. Live fish can coordinate their body motions in harmony with the surrounding fluid generating large transient forces efficiently, as opposed to rigid hull underwater vehicles (UV) powered by rotary propellers [1–2]. For a man-made vehicle

R.J. Clapham (✉) · H. Hu
School of Computer Science and Electronic Engineering, University of Essex, Colchester CO4 3SQ UK
e-mail: r.j.c@ieee.org; richard.j.clapham@gmail.com
URL: http://www.isplash-robotics.com

H. Hu
e-mail: hhu@essex.ac.uk

R. Du et al. (eds.), *Robot Fish*, Springer Tracts in Mechanical Engineering,
DOI 10.1007/978-3-662-46870-8_7

to achieve greater locomotive capability there is potential to engineer a structure that can accurately replicate the wave form of swimming fish.

Bainbridge's intensive observational studies measured live fish to attain an average maximum velocity of 10 body lengths/second (BL/s) [3]. A single high performance of a Cyprinus carpio was noted, achieving the swimming speed of 12.6 BL/s (1.7 m/s) with a distance traveled per tail beat or Swimming number (Sw) of 0.7. Endurance at the highest velocities is limited, burst speeds can only be maintained for short durations of approximately one second. Velocities were measured to decrease to 7 BL/s in 2.5 s of swimming, to 5 BL/s in 10 s, and to 4 BL/s in 20 s.

Although engineers have focused on hydrodynamic mechanisms, currently published robotic fish are unable to gain the locomotive efficiencies of live fish, proving a complex challenge. There are two limitations in particular: (i) They cannot achieve accurate replication of the linear swimming motion as free swimming robotic fish generate kinematic parameter errors and therefore reduced propulsion; (ii) They have low force transfer due to the complexity of developing the power train, limited by mass, volume, force, frequencies, and internal mechanical losses. Some examples of novel design approaches and their maximum velocities are Barrett's hyper-redundant Robotuna, achieving a maximum velocity of 0.65 body lengths/second (BL/s) (0.7 m/s) [4], Anderson's VCUUV with 0.5 BL/s (1.2 m/s) [5], Yu's discrete structure with 0.8 BL/s (0.32 m/s) [6], Essex's G9 with 1.02 BL/s (0.5 m/s) [7], Wen's carangiform with 0.98 BL/s (0.58 m/s) [8], and Valdivia y Alvarado's compliant method with 1.1 BL/s (0.32 m/s) [9]. The straight line speed of current robotic fish, peaking at 1 BL/s, is typically unpractical for marine-based environments.

In particular the kinematic errors are due to the lateral (F_L) and thrust (F_T) forces not being optimized and as a consequence excessive anterior destabilization in the yaw plane due to the concentration of posterior thrust creates reaction forces around the center of mass [7, 9]. In turn the anterior creates posterior displacement errors. As a result the body wave motion along the full length of body has large matching errors in comparison to the swimming patterns of live fish leading to reduced performance and high cost of transport.

Research Objectives This research project considered the factors contributing to the linear swimming speed of current robotic fish and initially proposed four main objectives: (i) to introduce a new swimming pattern to reduce the kinematic parameter errors by coordinating transverse displacements along the body length; (ii) to allow for efficient energy transfer by engineering a mechanism that takes into account hardware and material constraints so that propulsion is not restricted; (iii) to develop a prototype to improve stability in the vertical and specifically the horizontal plane, by optimizing the lateral and thrust forces around the center of mass; and (iv) to validate the proposed swimming motion by realizing a mechanism capable of consistent free swimming operation, measuring its achievement in terms of speed, thrust, and energy consumption over a range of frequencies.

The remainder of the chapter is organized as follows: Sect. 2 presents the design, construction, and experimental results of the first generation prototype, namely

iSplash-I, and introduces a new approach to coordinated full-body length swimming motion. Section 3 describes the new mechanical drive system and fabrication technique and experimental results of the second generation, *iSplash*-II. Finally, a brief conclusion and future work are given in Sect. 4.

2 *iSplash*-I: A New Robotic Fish with Full-Body Coordination

2.1 Design Methodology

Traditional Approach Modeling from body and/or caudal fin (BCF) swimmers, the selected carangiform swimming mode can be identified by the wave length and amplitude envelope. The Cyprinus carpio (common carp) has been chosen specifically for its high locomotive performance [3, 10].

We only consider modeling within the confinements of the horizontal plane where the kinematics of propulsion is commonly reduced to the form of a traveling wave, concentrated to the posterior, varying in amplitude along the length, smoothly increasing toward the tail [2]. Present robotic swimmers adopted this method which limits undulatory motions, typically to <1/2 the body length toward the posterior and the wave form motion consists of one positive phase and one negative phase. The commonly adopted model proposed in [4], is in the form of:

$$y_{\text{body}}(x,\ t) = \left(c_1 x + c_2 x^2\right)\sin(kx + \omega t) \tag{1}$$

where y_{body} is the transverse displacement of the body; x is the displacement along the main axis starting from the nose of the robotic fish; $k = 2\pi/\lambda$ is the wave number; λ is the body wave length; $\omega = 2\pi f$ is the body wave frequency; c_1 is the linear wave amplitude envelope, and c_2 is the quadratic wave. The parameters $P = \{c_1, c_2, k, \omega\}$ can be adjusted to achieve the desired posterior swimming pattern.

Proposed Full-Body Swimming Motion Propulsion of carangiform swimming is associated with the method of added mass [11]. Each propulsive segment of the traveling wave creates a force against the surrounding water generating momentum. This causes a reaction force (F_R) from water onto the propulsive segment. F_R normal to the propulsive segment is decomposed into the lateral F_L component which can lead to energy loss and anterior destabilization and the thrust F_T component providing propulsion increases in magnitude toward the tail. The overall magnitude of added mass passing downstream is approximately measured as the water mass accelerated and its acceleration (Fig. 1).

Therefore, it is proposed that initiating the starting moment of added mass upstream and optimizing the F_L and F_T forces around the center of mass would increase the overall magnitude of thrust contributing to increased forward velocity. In consideration of this, we designed a novel robotic fish which can operate in two

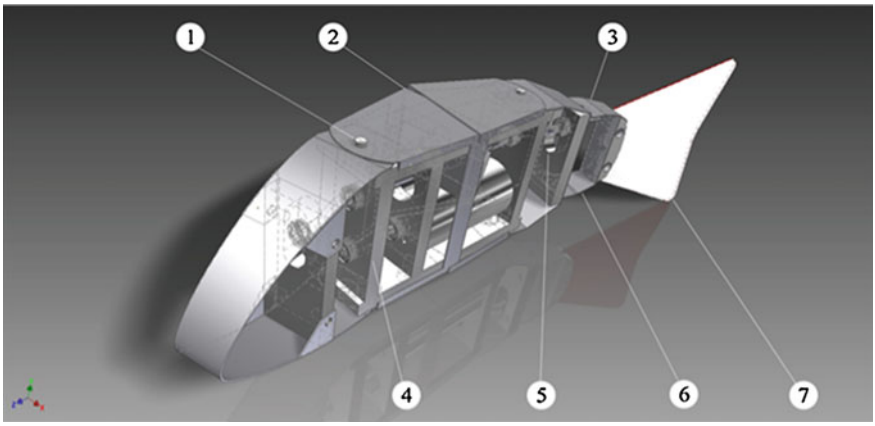

Fig. 1 *iSplash*-I: *1* Anterior joint; *2* Mid-body links; *3* Posterior with thick peduncle; *4* Transmission system; *5* Driven tail plate; *6* Tendons; *7* Compliant fin

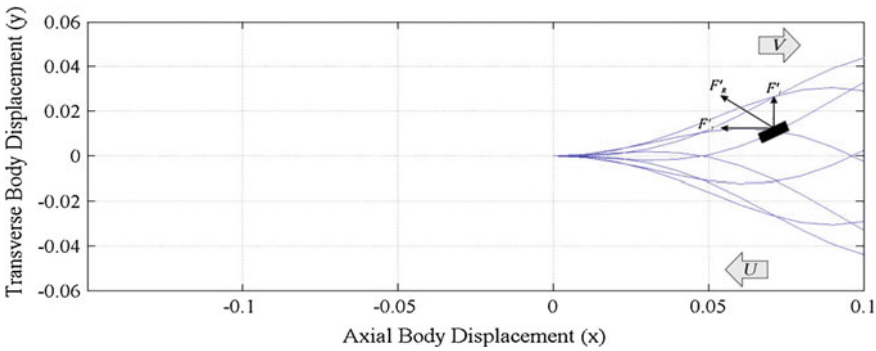

Fig. 2 Mode 1: Wave form is confined to the posterior 2/5. Parameters have been determined from experimental tests. Showing the thrust generation by the method of added mass (Adapted from Webb [11])

swimming patterns: (i) Applying a traditional rigid mid-body and anterior. Concentrating the undulations and degrees of freedom (DOF) to the posterior end of the body length which will be described as Mode 1, illustrated in Fig. 2; (ii) Based on intensive observation and fluid flow assumptions a new full-body carangiform swimming pattern is introduced. The coordination of anterior, mid-body, and posterior body motions are proposed in an attempt to reduce kinematic parameter errors, this will be described as Mode 2, illustrated in Fig. 3.

The models midline and body motion parameters were first established based on observation and published data from literature providing an initial engineering reference. The wave form motion first developed for a discrete rigid anterior

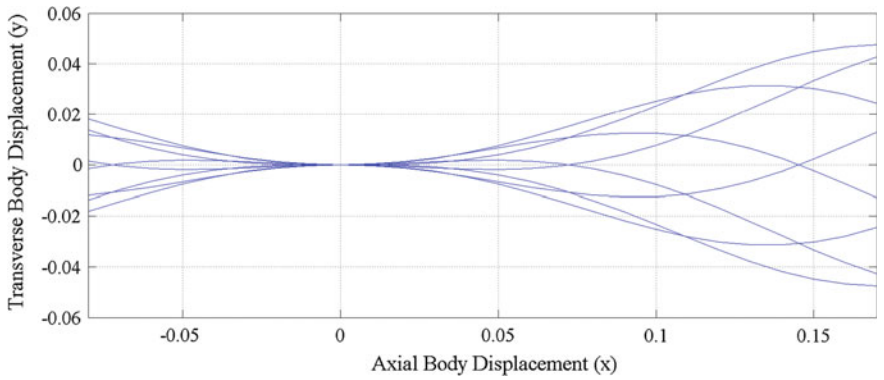

Fig. 3 Mode 2: Full-body coordination. The kinematic parameters have been determined from experimental tests

prototype in [7] can be extended to represent the full-body motions of Mode 2 in the form:

$$y_{\text{body}}(x,t) = \left(c_1 x + c_2 x^2\right) \sin(\text{k}x + \omega t) - c_1 x \sin(\omega t) \tag{2}$$

The relationships between the defined parameters $P = \{0.44, 0, 21.6, 8\}$ shown in Fig. 3 can first be found by evaluating the x location pivot at 0. In the kinematic pattern of Mode 2, the fraction of body length displaced is equal to the anguilliform swimming mode but reflects changes in the wave form. The anguilliform swim pattern is defined by large amplitude undulations propagating from nose to tail. The newly introduced Mode 2 applies an oscillatory motion to head and mid-body and pivots the entire body around a single point associated with the carangiform fish swimming motion [2].

Although this is the first account of applying full-body actuation to a research prototype fish, mechanisms such as "vortex peg" and "undulating pump" and flow visualization techniques have been proposed [12, 13] from published biological studies, indicating a possible fluid body interaction that contributes to propulsive thrust is generated upstream to the posterior section. The muscle activity in the anterior has been measured to be low, suggesting that accurate modeling of the kinematics could be more significant than anterior force in improving energy transfer.

As previously mentioned, anterior destabilization has been difficult to control [6, 7, 9], as passive rigid anterior mechanisms recoil around the center of mass. Free swimming robotic fish have excessive head swing, similar in magnitude to the posterior which increases drag. The proposed Mode 2 drives the anterior into the unwanted yaw direction, in an attempt to reduce amplitude errors by optimizing the F_R around the center of mass. It has also been noted in [2], that the morphological adaptations of reduced depth at the peduncle, increased depth of body toward the anterior and vertical compression minimize recoil forces.

2.2 Construction Method

Mechanical Design Mechanical structure limitations set a great challenge when modeling the displacements within the traveling wave. Current methods typically adopt either a discrete assembly [6, 7] or compliant structure [9] but both are seen to have limitations. A construction method using structural compliance combined with a rigid discrete assembly is proposed. The arrangement distributes three actuated joints and one coupled joint along the axial length shown in Fig. 4.

Mode 1 disregards transverse displacements of links I, II, III whereas Mode 2 actuates all links along the axial length to provide anterior and mid-body transversal displacements. The development allowed for both Modes of operation to be applied to the same prototype by adjusting the configuration. Uniform material properties were chosen for links I–III and stiffness distribution begins at joint 3 and continues to the tail tip. To provide the undulatory motion a compliant caudal fin is attached to the link V and is actuated by tendons anchored to the main housing rear bulkhead. The developed mechanism allows for the expansion of the tendons and material stiffness of the caudal fin to be adjusted experimentally to provide the targeted curves during free swimming at various frequencies.

The approximation of a traveling wave using links I–V and turning angles of joints 1–4 are shown in Fig. 4. Details of the fully discretized body wave fitting method are given in [6, 7]. The location of joints in the series can be determined by parameterized fitment to a spatial and time dependent body wave. The discrete

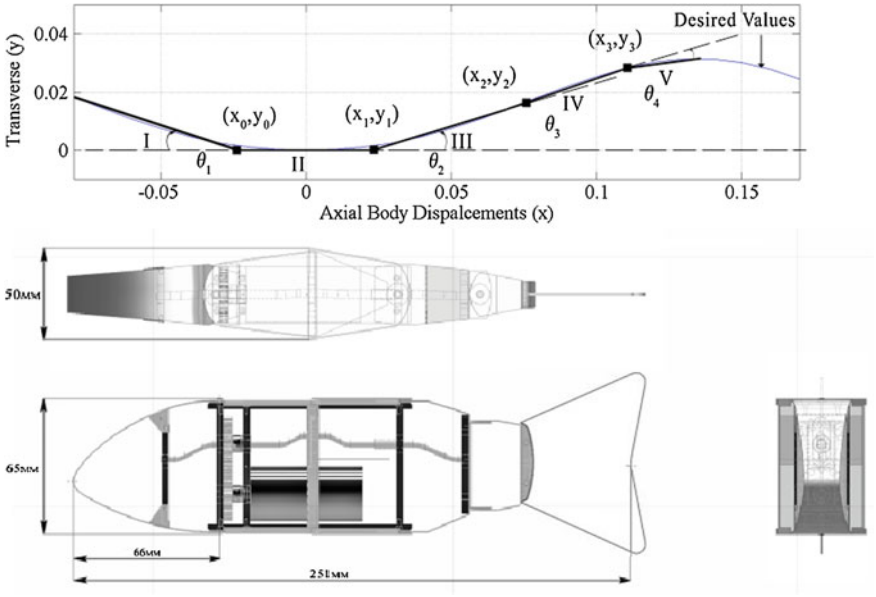

Fig. 4 Link approximation (*top*); *1* Plan; *2* Profile; *3* Front (*bottom*)

construction method can be defined as a series of links or N links. N being the number of links after joint 1 typically <6 due to structural limitations, more links reduce curve alignment errors. The aim of the design is to improve complexity of motion without an increase of structural parts. The link end points are shown in Fig. 4, it can be seen that the arrangement of links distributed along the length of the body provides an accurate curve alignment reducing large errors and excrescences in the outer profile. In addition we have observed that the aerofoil section NACA (12)520 based on camber, chord, and thickness can be utilized to illustrate the outer structure profile of Mode 2, which we propose contributes to the fluid flow interaction.

Power Transmission System The developed transmission system providing rotary power to linear oscillations is illustrated in Figs. 5 and 6. All actuated links are directly driven by the five-bearing crankshaft providing an equal power distribution. The developed mechanical design required high-precision engineering of the chassis and crankshaft to avoid deadlock and reduce friction. The driven link amplitudes are determined by the offset cranks, L_3 represents one of the discrete links of the structure. The maximum amplitude of the link length L_3 at point P_2 is determined by the predetermined maximum crank offset P_1. The coordinates of P_1 (P_{1x}, P_{1y}) and P_2 (P_{2x}, P_{2y}) can be derived by:

$$\begin{cases} P_{1x} = A + B\cos\theta_1 + C\cos\theta_2 \\ P_{1y} = B\sin\theta_1 + C\sin\theta_2 \end{cases} \begin{cases} P_{2x} = P_{1x} + D\sin\theta_2 \\ P_{2y} = P_{1y} + D\sin\theta_2 \end{cases} \tag{3}$$

The length of L_3 can be derived by $L_3^2 = P_{2x}^2 + P_{2y}^2$. Assume that ω_1 is the angular velocity of the link L_3, and the velocity vector V_{P2} is perpendicular to L_3. We have:

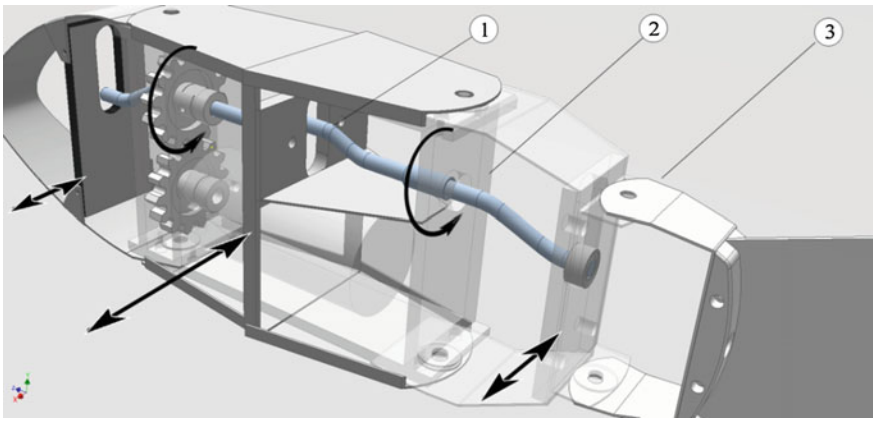

Fig. 5 Power transmission system: *1* Transision plate; *2* Crankshaft; *3* Free end of link and connecting pivot

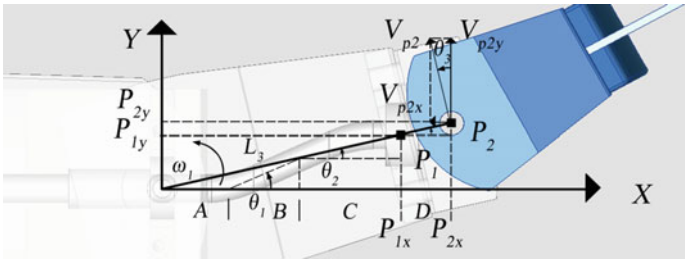

Fig. 6 Schematic drawing of the tail offset drive crank and linkage

$$\begin{cases} V_{p2x} = -\omega_1 L_3 \sin\theta_3 \\ V_{p2y} = \omega_1 L_3 \cos\theta_3 \end{cases} \tag{4}$$

where V_{p2x} and V_{p2y} are the decomposed vectors of the velocity vector $V_{P2} = \omega_1 L_1$.

Fabrication *iSplash*-I shown in Fig. 7 was engineered as a morphological approximation of the common carp. The physical specifications are given in Table 1. We devised a structurally robust prototype allowing for consistency of operation at high frequencies, as force has to be applied to the water and reactively, the opposing force is applied to the vehicle. All structural parts were precision engineered, hand fitted, and assembled. A consideration of the development took hardware and material constraints into account, so that geometric and kinematic parameters are not affected. The hydrostatic streamlined profile was optimized

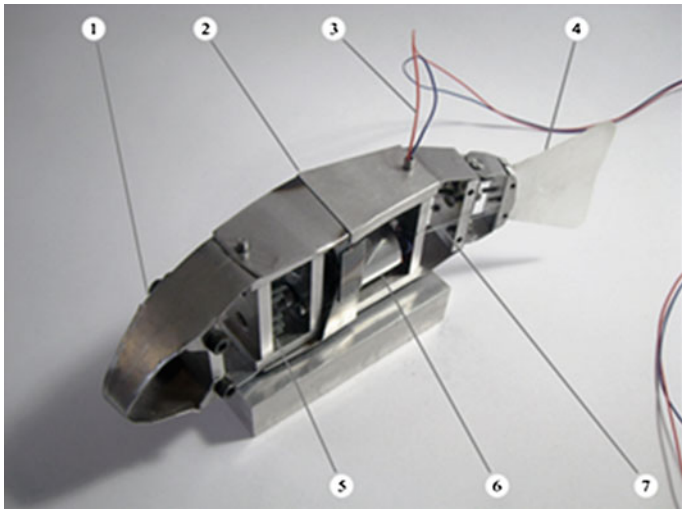

Fig. 7 Inner Structure of *iSplash*: *1* Steel space frame; *2* Mid-body driven plate; *3* External source cables; *4* Polypropylene caudal fin; *5* Aluminum main bulkhead; *6* Electric motor; *7* Offset crankshaft

Table 1 Physical parameters of *iSplash*-I

Parameters	Specific value
Body size: m (L × W × H)	0.25 × 0.05 × 0.062
Body mass (Kg)	0.367
Maximum velocity BL/s (m/s)	3.4 (0.88)
No-load maximum frequency (Hz)	8
Actuator	Single electric motor
Power supply	12 V Pb external battery supply
Fabrication	Low tolerance engineering
Materials	Aluminum, mild steel, stainless
Swimming mode	Linear locomotion
Tail material	Polypropylene
Outer structure and skin material	Polystyrene and polypropylene
Caudal fin aspect ratio (AR)	1.73

by favorably positioning the maximum thickness of the cross section, reducing pressure drag. In [10], the cross section has been measured to be optimal at 0.2 of the body length. These aspects relate to amount of resistance during forward motion and were taken into consideration within the design.

Increasing endurance is a desirable feature of a UV. Current robotic fish are still limited to short operational times as energy losses can be produced in many stages of the mechanical transfer. Recent designs have found that it is advantageous to utilize a single electrical motor for actuation [9]. The classical actuator is still the most effective way of providing power at high frequencies and reduces energy consumption over multilink discrete assemblies. Mass and volume distribution are key principles of stability in the horizontal and vertical planes. A single actuator power transmission system can be positioned in the optimum location. In contrast multilink servo assemblies are limited as mass and volume are confined to the posterior (Table 2).

Table 2 Comparison of test results between Modes 1 and 2

Parameters	Mode 1	Mode 2
Reynolds number Re (10^5)	1.4	1.7
Strouhal number (St)	0.48	0.41
Maximum thrust (N)	0.63	1.17
Consistent maximum velocity BL/s (m/s)	2.2 (0.55)	2.8 (0.70)
Frequency (Hz)	6.1	6.6
Max power consumption air (W)	3.48	3.76
Max power consumption water (W)	5.76	7.68
Swimming number (Sw)	0.36	0.42
Head swing amplitude (m)	0.044	0.018
Tail swing amplitude (m)	0.044	0.044
Test run distance (m)	0.5	0.5

The body has open-loop stability if the relative position of buoyancy is higher than the center of mass as the surrounding fluid counterbalances the gravitational weight [14]. Therefore, the hydrostatic buoyancy level and stability were solved by adjusting material properties and configuration. Stability was found to be particularly difficult to maintain during free swimming at high frequencies.

Lastly, the inner structure of the prototype is negatively buoyant. A significant development of the prototype was a watertight skin that allowed unrestricted flexing of the external surface and provided the volume needed to maintain neutral buoyancy.

2.3 Experimental Procedure and Results

Field Trials A series of experiments were undertaken in order to verify the proposed swimming pattern by assessing the locomotive performance of Modes 1 and 2 in terms of speed, thrust, and energy consumption at frequencies in the range of 2–8 Hz. Experiments were conducted within a 1 m long × 0.5 m wide × 0.25 m deep test tank. Stabilized free swimming over a distance of 0.5 m was used to measure speed with a 0.5 m acceleration distance. The prototype had sufficient space to move without disturbances from side boundaries and the free surface. Measurements were averaged over many cycles once consistency of operation was achieved and steady state swimming was obtained.

Although the prototype was measured to have a higher mechanical efficiency with an oil-filled structure, the developed skin proved inconsistent. Therefore, all runs were completed actuating the prototype with a water filled structure. This method attained consistency of operation providing stabilized swimming and maintaining the required buoyancy within the depth of the testing tank, whilst gently skimming the bottom surface. Velocity greatly reduced during runs when the skin detached, the build became negatively buoyant, destabilized, or the cross-sectional area was increased.

Swimming Pattern Observation Figure 8 shows snapshots of Mode 2 in eight instances with time intervals of 0.02 s throughout one body cycle. The midline was tracked at 50 frames per second to provide the amplitude envelopes of the anterior and posterior for comparison. Good agreement with fish kinematic data is a difficult task and current free swimming robotic fish have shown excessive head and tail amplitude errors. When comparing Modes 1 and 2, Mode 2 was found to reduce the head amplitude by over half from 0.17 (0.044 m) of the body length in Mode 1 to 0.07 (0.018 m). The tail amplitude of the common carp is 0.1 [3, 10], larger values were found to increase performance. Both Modes 1 and 2 were able to attain amplitudes of 0.17 (0.044 m). The location of the midline pivot point should be in the range of 0.15–0.25 of the body length [10]. Mode 2 has a reduced error location of 0.33 in comparison to 0.5 in Mode 1. Indicating Mode 2 greatly reduces the kinematic matching errors.

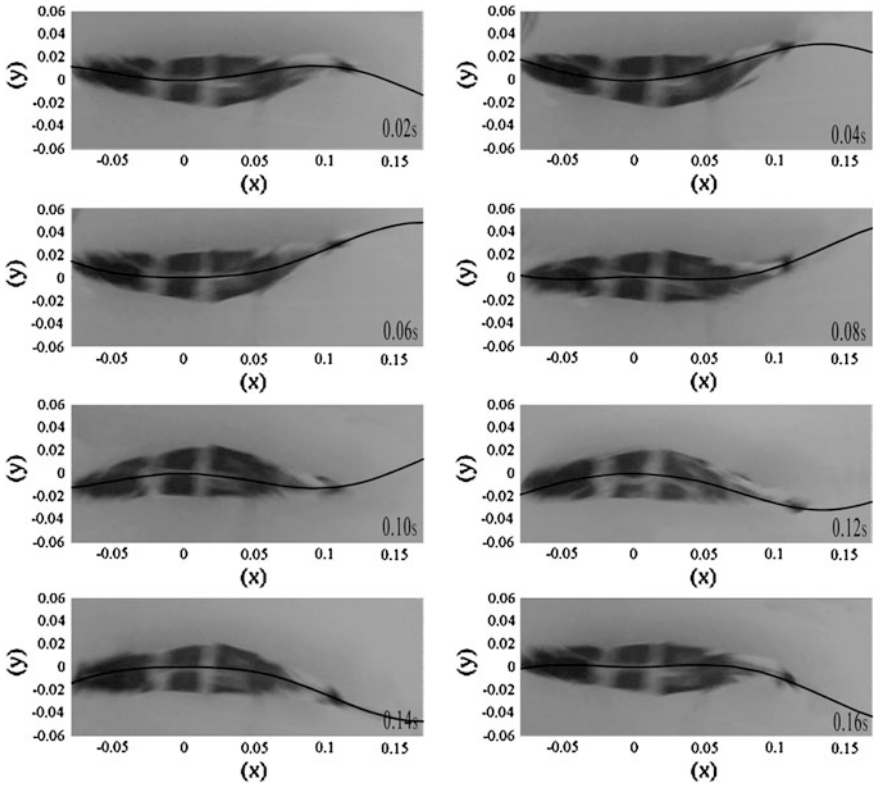

Fig. 8 Mode 2 during one body cycle, eight instances every 0.02 s

In addition it was observed that the posterior 2/5 of the body length deforms due to stiffness distribution providing a smooth transition phase between body and tail. Although high aspect ratio (AR) caudal fins have been found to produce greater efficiency [15], in initial testing a low aspect ratio tail provided higher speeds. AR is calculated using: AR = b^2/Sc where b squared is the fin span and Sc is the projected fin area. AR in this case was 1.73.

Experimental Results Figure 9 shows the average energy consumption in relationship to driven frequency, comparing both Modes in air and water. This comparison measured the value of the increased resistance during locomotion due to the surrounding liquid. Measuring of energy consumption and thrust took many cycles to average, as the swimming motion produces fluctuating readings within a single body motion cycle. Both Modes actuating in water resulted in an increase in energy consumption, i.e., Mode 2 increasing from 3.76 to 7.68 W and Mode 1 increasing from 3.48 to 5.76 W.

As the configurations of robotic fish show various hardware and morphological properties, the main value of comparison has become speed divided by body length

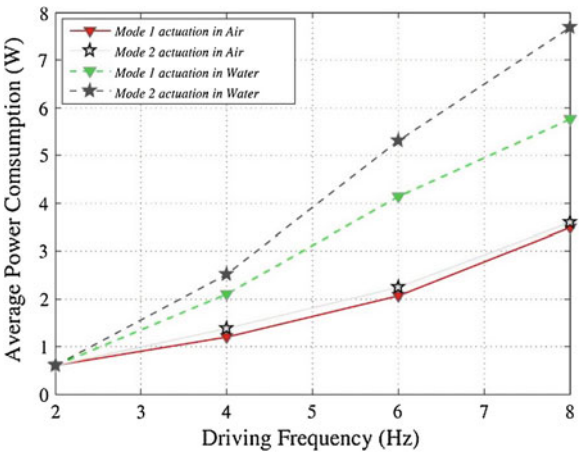

Fig. 9 Comparison of average electrical power consumption over driven frequency of both Modes, actuating in air and water

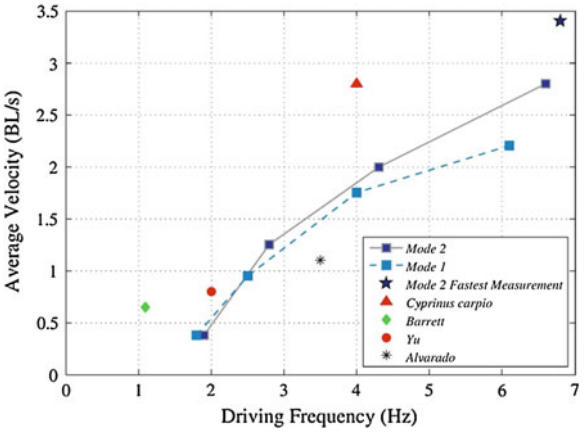

Fig. 10 Comparison of average velocities achieved by both modes, contrasted against current robotic fish and the cruising speed of a real common carp

(BL/s). In this case the body length is measured from nose tip to the most posterior extremity of the tail.

The relationship between velocity and driven frequency is shown in Fig. 10. The corresponding values of Modes 1 and 2 during consistent swimming were measured and compared to current robotic fish. Mode 1 achieved maximum velocity of 2.2 Bl/s (0.55 m/s), at 6.1 Hz. Mode 2 increased maximum velocity to 2.8 BL/s (0.70 m/s) at 6.6 Hz. Mode 2 has an increased performance in comparison with current robotic fish which typically peak around 1 BL/s. An initial value of 3.4 BL/s (0.87 m/s) at 6.8 Hz was recorded by Mode 2 with an oil-filled structure. Sealing the developed skin when in contact with oil could not be maintained and skin detachment consistently affected stability and buoyancy, greatly reducing performance.

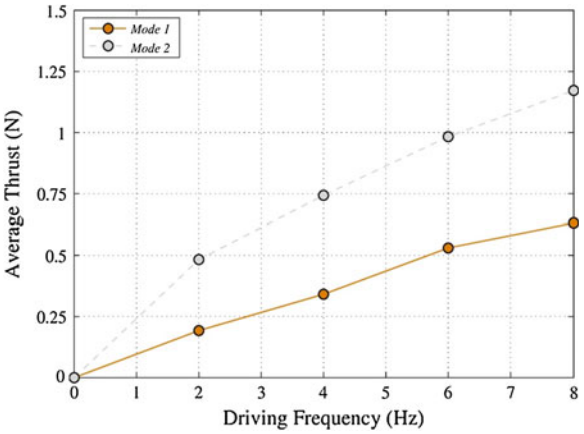

Fig. 11 Comparison of average thrust in relationship to driven frequency achieved by both Modes

We can notice that Mode 2 had an 85 % increase of thrust (Fig. 11) and a 27 % increase in velocity over Mode 1 whilst consuming only 7.68 W of power at 2.8 BL/s. As the power supply contributes to a significant portion of the total mass, high energy efficiency is important. The measured low energy consumption indicates that the next generation could carry its own power supply within a comparable geometric frame with good endurance.

A prominent parameter for analyzing BCF locomotive performance is the Strouhal number (St), defined as $St = fA/U$, *w*here f denotes the frequency, A denotes the tail amplitude, and U is the average forward velocity. St is considered optimal within the range of $0.25 < St < 0.40$. Mode 1 has a peak St of 0.48 under the condition of $Re = 1.4 \times 10^5$ and Mode 2 consistently measured a St = 0.41 and peaked at a St = 0.34 under a condition of $Re = 2.2 \times 10^5$. A comparable live fish was measured in [16], to have a St = 0.34, $Re = 2 \sim 8 \times 10^5$. Applying Mode 2 shows a high-performance increase within the St optimal range and achieves the higher cruising speeds of swimming fish.

A significant relationship between velocity and driven frequency was found. As higher frequencies were applied velocity increased in both Modes, matching the reported findings of live fish [3]. From this it can be assumed that a further increase of frequency applied to this prototype may continue to increase its performance.

3 *iSplash*-II: Realizing Fast Carangiform Swimming

As previously noted, throughout the field trials *iSplash*-I was able to replicate the key swimming properties of real fish. As frequencies were raised the prototype continued to increase velocity. This matches Bainbridge's study of swimming fish, measuring no noticeable change in kinematics after tail oscillations are raised beyond 5 Hz, indicating that only an altered frequency is required to increase

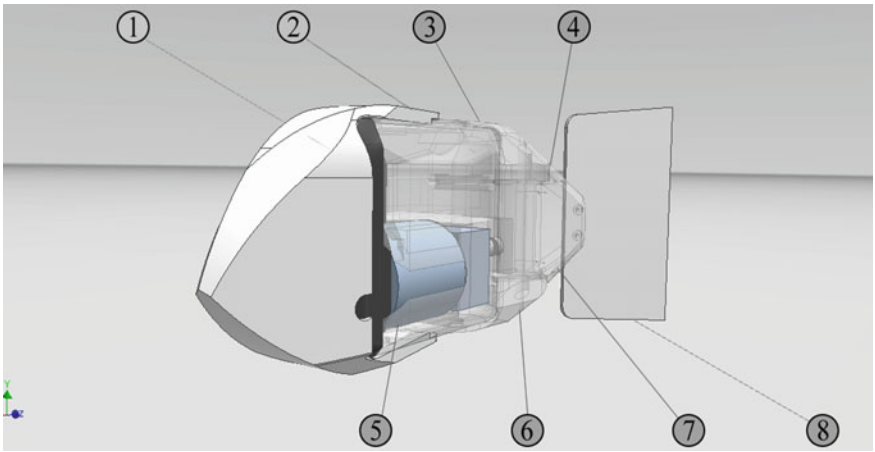

Fig. 12 *iSplash*-II: *1* Anterior link; *2* Mid-body transition links; *3* First posterior link; *4* Final posterior pivot; *5* Primary actuator; *6* Direct drive offset crank; *7* Tendon driven peduncle; *8* Compliant caudal fin

swimming speed. Hence it was expected, that combining the critical aspects of the *iSplash*-I mechanical drive system with frequencies higher than 6.6 Hz may significantly increase maximum velocity, *iSplash*-II was developed.

Figure 12 presents *iSplash*-II, a prototype 32 cm in length which has achieved consistent untethered stabilized swimming speeds of 11.6 BL/s (i.e., 3.7 m/s), with a frequency of 20 Hz. The prototype was developed with a new fabrication technique and mechanical drive system, effectively transmitting large forces at high frequencies to obtain high-speed propulsion. The F_L and F_T forces were optimized around the center of mass, generating accurate kinematic displacements and increasing the magnitude of added mass.

Research Objectives This prototype was developed with the aim of achieving the fastest swimming speeds of real fish with seven main objectives:

(i) to devise a prototype which operates in the two swimming patterns, for further investigation of the carangiform swimming motion to be conducted;
(ii) to significantly increase force transfer by achieving a high power density ratio in combination with an efficient mechanical energy transfer;
(iii) to achieve unrestricted high force swimming by realizing a prototype capable of carrying a high powered energy supply;
(iv) to develop a structurally robust mechanical drive system based on the critical properties proposed in [17], capable of intensively high frequencies of 20 Hz;
(v) to greatly reduce forward resistance by engineering a streamlined body considering individual parts' geometries and alignment throughout the kinematic cycle;

(vi) to stabilize the free swimming prototype's unsteady oscillatory motion during intensively high frequencies to achieve a more efficient force transfer;
(vii) to conduct a series of experiments measuring the prototype's achievements in terms of kinematic data, speed, thrust, and energy consumption in relation to driven frequency.

3.1 Construction Method

Mechanical Design In order to increase the swimming speed a new mechanical drive system was required, able to effectively transmit large forces at intensively high tail oscillation frequencies. In consideration of this, a feasible design structure to fit the linear swimming patterns of both modes was developed. Although a power train utilizing a single motor with continuous rotation is more complex to develop without large internal mechanical loss [4], it is still advantageous in comparison to multilink servos or smart materials, which are limited by force, frequency, volume, and mass distribution [6–8]. Therefore a single actuator was deployed, as shown in Fig. 13.

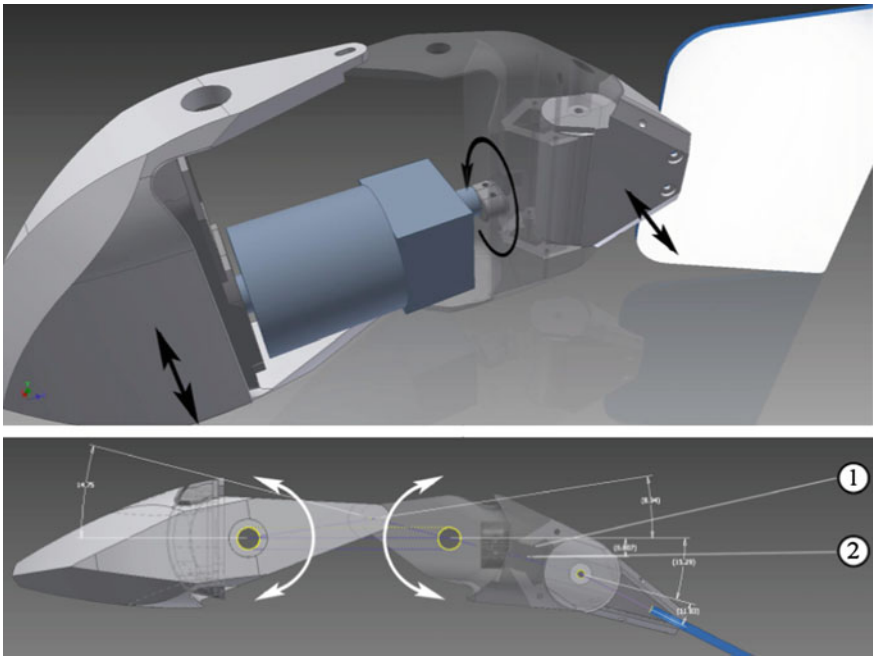

Fig. 13 Power transmission system: *1* Offset crank; *2* Posterior link

As the build required a high power density ratio, the structural arrangement was governed by the dimensions of the large electrical motor 83 mm long × 50 mm diameter. This required a slight increase in body length from 250 mm to 320 mm and a significant adjustment to the link structure to take the mass of the actuator into consideration, removing the coupled mid-body joint and the associated discrete linkages. The discrete construction method, defined as a series of links or N links, aims to achieve accurate midline kinematic parameters whilst minimizing complexity of the mechanical drive and linkages. The sequence of links can generate the required swimming motion by locating the joints to the spatial and time-dependent body wave. The fully discretized body wave fitting method is given in [6, 7].

The assembly of *iSplash*-II is illustrated in Fig. 14, showing the four joints distributed along the axial length. Three rigid links are coupled to a compliant fourth link and caudal fin with stiffness distribution, devised to generate a smooth body to tail transition phase of the posterior undulations. The developed modular build allowed for both Modes of operation to be applied to the same prototype by adjusting the configuration. Links III and IV are actuated to generate the posterior kinematics of operational Mode 1, Mode 2 actuates all links along the axial length to provide anterior, mid, and posterior body displacements.

It was proposed in [17], that the outer profile of the coordinated full-body swimming pattern, represented by the aerofoil section NACA (12)520 aids the fluid flow interaction, producing greater locomotive speeds. In consideration of the simplified link assembly and estimated center of mass, the head and tail amplitudes were increased. As can be seen in Fig. 15, the approximation of a traveling wave

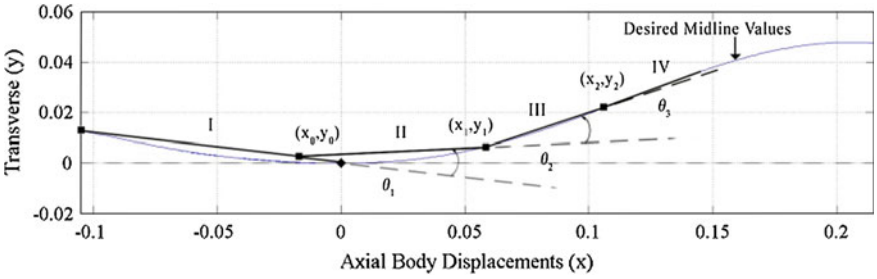

Fig. 14 Link approximation, illustrating accurate kinematic matching

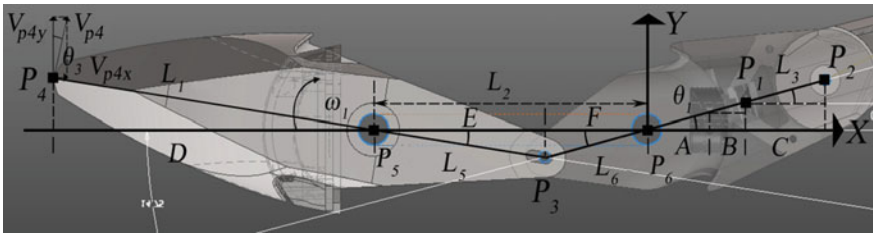

Fig. 15 Schematic drawing of the offset drive crank and linkages

using link end points I–IV and turning angles of joints 1–3 of the reduced link arrangement provides an accurate curve alignment agreeable with the form of (2), therefore reducing errors and excrescences in the outer profile and achieving accuracy with the required aerofoil section.

Power Transmission System The leading tail discrete link III is directly driven by the single bearing crankshaft attached to the output shaft of the primary actuator, increasing power distribution to the posterior. As link III is actuated, link IV is passively displaced. This final posterior linkage IV, coupled to the compliant caudal fin is anchored by four expandable tendons attached to the main chassis rear bulkhead, crossing through linkage III. The anterior link I is transmitted motion by paired linkages fixed at points P_5 and P_6, located at the top and bottom of the main chassis. The developed mechanical design required precision fitment of the chassis, crankshaft, cantilevers, and linkages to reduce internal mechanical losses, avoid deadlock, and reduce friction.

Illustrated in Figs. 13, 14, and 15 is the developed power train transmitting rotary power to linear oscillating links. All driven link amplitudes are determined by the single offset crank. L_3 represents the leading tail discrete link of the structure.

The maximum amplitude of the link length L_3 and L_1 at point P_2 and P_4, respectively, are determined by the predetermined maximum crank offset P_1. The coordinates of P_1 (P_{1x}, P_{1y}), P_2 (P_{2x}, P_{2y}), P_3 (P_{3x}, P_{3y}), and P_4 (P_{4x}, P_{4y}) can be derived by:

$$\begin{cases} P_{1x} = A + B \\ P_{1y} = (A + B)\tan\theta_1 \end{cases} \begin{cases} P_{2x} = P_{1x} + C\cos\theta_1 \\ P_{2y} = P_{1y} + C\sin\theta_1 \end{cases} \tag{5}$$

$$\begin{cases} P_{3x} = -F\cos\theta_1 \\ P_{3y} = -F\sin\theta_1 \end{cases} \quad \begin{cases} P_{4x} = -(L_2 + D) \\ P_{4y} = -P_{3y}D/E \end{cases} \tag{6}$$

The length of L_1 can be derived by $L_1^2 = P_{4x}^2 + P_{4y}^2$. Assume that ω_1 is the angular velocity of the link L_1, and the velocity vector V_{P4} is perpendicular to L_1. We have:

$$\begin{cases} V_{p4x} = -\omega L_1 \sin\theta_3 \\ V_{p4y} = \omega L_1 \cos\theta_3 \end{cases} \tag{7}$$

where V_{p4x} and V_{p4y} are the decomposed vectors of the velocity vector $V_{P4} = \omega_1 L_1$.

Fabrication The prototype *iSplash*-II is shown in Fig. 16 with the physical specifications given in Table 3. The entire body was digital modeled and formed using 3D printing techniques, at layers of 0.09 mm in PLA filament. This method produced precise 3D structural geometries of the individual segments and predetermining alignment tolerances throughout the complete kinematic cycle. It was a key challenge to develop a high power density build, small in size with high structural strength. The individual printed parts were optimized for robustness through physical strength tests and computational stress analysis, highlighting

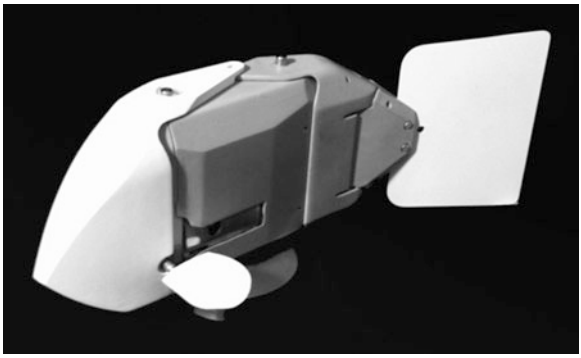

Fig. 16 *iSplash*-II

Table 3 Physical parameters of *iSplash*-II

Parameters	Specific value
Body size: m (L × W × H)	0.32 × 0.048 × 0.112
Body mass (Kg)	0.835
Actuator	Single electric motor
Actuator mass (Kg)	0.63
Power supply	11.1 V onboard LiPo battery
Manufacturing technique	3D Printing
Materials	PLA filament, acetal, stainless
Primary swimming mode	Linear locomotion
Additional maneuverability	Vertical plane
Additional control surfaces	Pectoral fins
Caudal fin material	Polypropylene
Thickness of caudal fin (mm)	2.3
Caudal fin aspect ratio (AR)	1.6

initial areas of weakness. These parts were reprinted many times in order to realize high frequency actuation. As PLA filament has a low melting point softening at approximately 60 °C, material wear at the pivots and actuated surfaces was reduced by acetal bushes and inserts, at the cost of additional weight.

It was necessary for the body size to be compact, as increasing the build geometric magnitude will increase the resistance during forward motion and therefore the power consumption required [4–17]. An accurate approximation of the streamlined body shape of the common carp was achieved within the horizontal plane illustrated in Fig. 13. The maximum thickness of the cross section is measured optimal at 0.2 of the body length [10] and was favorably positioned therefore reducing pressure drag.

The static stability in the horizontal and vertical planes is affected by material density distribution. For linear locomotive research open-loop stability is beneficial, this was achieved by the relative position of buoyancy being higher than the center

of mass, as the surrounding fluid counterbalances the gravitational weight [14]. The short body length greatly increased the difficulty in achieving open-loop stability as the finest weight change in structure of individual pieces distributed across the assembly dramatically affected stability and buoyancy. This was solved by collaborating the individual parts of the modular build by adjusting the geometries and the inner structure's weight to strength configuration.

The prototype was designed with increased stability in roll and pitch as the large mass of the electric motor, 0.6 kg, 75 % of the total mass, was positioned low within the structure. To achieve a short body length, contain the embedded system and 11.1 V LiPo power supply and counteract the large mass of the primary actuator the build volume was increased vertically. This aided stability, as the lightweight PLA material and increased height positioned the center of buoyancy at the top of the prototype.

Mobility within the vertical plane was achieved to maintain a stable mid-tank trajectory during free swimming. Two rigid morphological approximations of pectoral fins were developed and positioned at the leading bulk head of the main chassis, actuated by a single servo motor. A cross beam anchored on both sides of the centralized motor was formed to link, support, and actuate the control surfaces. The addition of pectoral fins required a compact mechanism to be devised due to the very restrictive space available.

3.2 Experimental Procedures and Results

Field Trials A series of experiments, identical to the first generation were conducted in order to verify the prototype by evaluating the locomotive performance of Modes 1 and 2 in terms of kinematic parameters, speed, force, and energy consumption at frequencies within the range of 5–20 Hz. In comparison to the tests of the first prototype the number of cycles was required to be raised to increase the accuracy of data. Measurements were taken once consistency of operation was achieved and stabilized free swimming was obtained. The test results are summarized in Table 4. Experiments were conducted within a test tank, 5 m long × 2 m wide × 1.5 m deep. Free swimming between two fixed points at a distance of 4 m was used to evaluate maximum speed. The prototype had sufficient space to move without disturbances from side boundaries and the free surface, capable of consistent untethered swimming at mid-height of the tank aided by adjusting the angle of pectoral fins during swimming.

Locomotion at high speeds was unachievable without extensive stability optimization. Once achieved, an accurate straight line trajectory was possible. A thorough description of the improvements undertaken on the mechanical structure and the extent of the intensive destabilization are beyond the scope of this chapter. In addition, the devised mechanical drive system was found to be very robust, showing no signs of structural failure throughout the field trials whilst

Table 4 Comparison of test results between Modes 1 and 2

Parameters	Mode 1	Mode 2
Maximum velocity BL/s (m/s)	11.6 (3.7)	11.6 (3.7)
Acceleration time to maximum velocity (s)	0.6	0.6
Frequency (Hz)	20	20
Reynolds number Re (10^6)	1.2	1.2
Strouhal number (St)	0.34	0.34
Maximum thrust (N)	9	9
Max power consumption air (W)	120	120
Max power consumption water (W)	120	120
Swimming number (Sw)	0.58	0.58
Head swing amplitude (m)	0.003	0.013
Tail swing amplitude (m)	0.063	0.063
Body length displaced (%)	51	76

actuating at intensively high frequencies over long periods and accidentally hitting the walls of the test tank.

Swimming Pattern Observation The frame sequence of Mode 2 in eight instances, at time intervals of 0.006 s throughout one complete body cycle at 19 Hz is illustrated in Fig. 17. The obtained midline was tracked at 50 frames per second and is plotted against the desired amplitude envelopes of the anterior and posterior for comparison. When observing the midline of Mode 2, it can be seen that the desired full-body coordination presented in [17] was not achieved. As previously described in Section III–A the build required a simplified link structure due to power density constraints. Although the estimated midline curve alignment tested during stationary actuation was accurate, the excessive mass of the primary actuator held the main chassis (the entire length of link II) fixed in line with the forward heading and no single pivot point was obtained. Consequently, the swimming motion during locomotion was found to produce matching errors over the full-body in comparison to the desired swimming pattern of *iSplash*-I.

Comparing both Modes, taking into consideration that the mid-body was held rigid, the anterior amplitude of Mode 2 was measured to be 0.04 (0.013 m) of the body length, equivalent to the common carp, whereas Mode 1 was found to generate <0.01 (0.003 m) head amplitude. In addition, the large centralized mass arrangement and increased depth of body effectively minimized recoil forces and aided the stability of the posterior, allowing for accurate posterior amplitude and large thrust forces to be generated.

Figure 18 shows that the developed posterior structure can accurately mimic the undulatory parameters of real fish, as the components of link IV can be adjusted experimentally to provide the targeted midline during free swimming at various frequencies. Both Modes were able to generate accurate amplitudes of 0.1 of the body length and attain large tail amplitudes of 0.2 (0.063 m) which was found to significantly increase performance. This value is twice the size of the observed

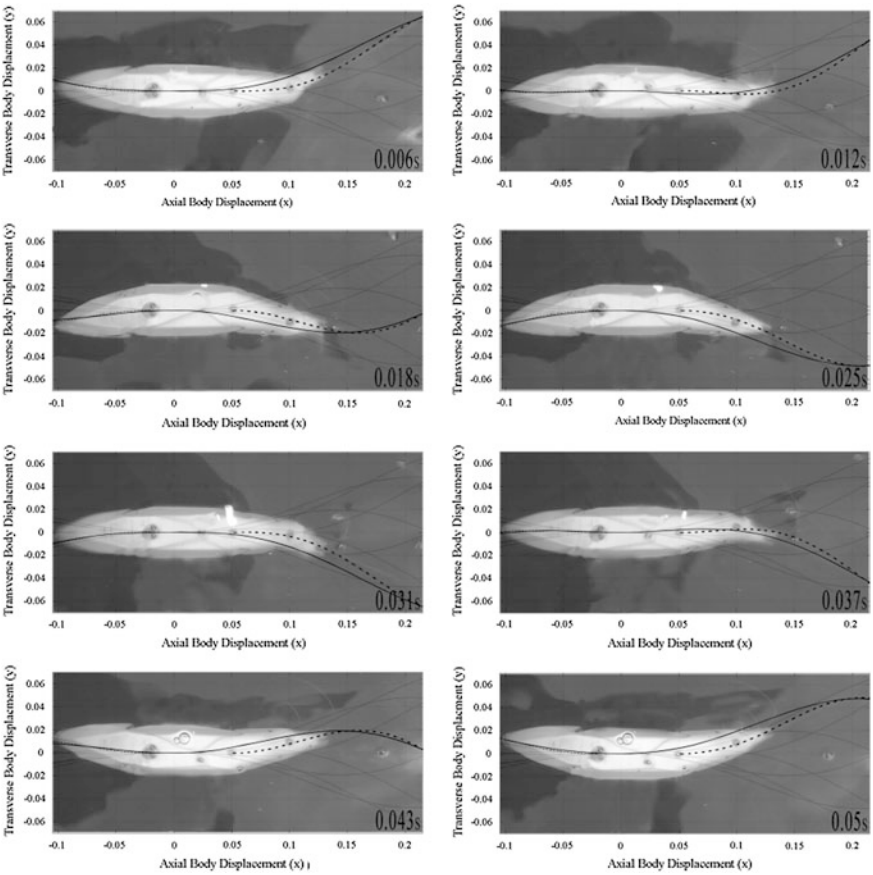

Fig. 17 Frame sequence of Mode 2 during one full-body cycle, eight instances every 0.006 s. The desired midline (—) (illustrated in Fig. 3) and the generated kinematics (illustrated in Fig. 2) from locomotion at 20 Hz (- -) are shown for comparison. We can see that the prototype achieved an anterior amplitude value of 0.04 L (0.013 m) and a tail amplitude value of 0.20 L (0.063 m)

value of the common carp at 0.1 and is increased over the first generation at 0.17. This generated amplitude is greater than the highly efficient swimming motion of a dolphin measured at 0.175 [10].

Replicating the form of the first generation the caudal fin was constructed with a low aspect ratio (AR). Although not yet thoroughly investigated, this tail was measured to achieve the highest maximum velocity and acceleration during the initial field trails. AR is defined as: AR = b^2/Sc where b squared is the fin span and Sc is the projected fin area. In this case the AR was 1.6.

Experimental Results In Fig. 18 the average energy economy in relationship to driven frequency is shown, comparing both operational Modes in air and water. It can be seen that both Modes actuating in water consumed a maximum 120 W at 20 Hz. This measurement was obtained by a connecting tethered power supply and

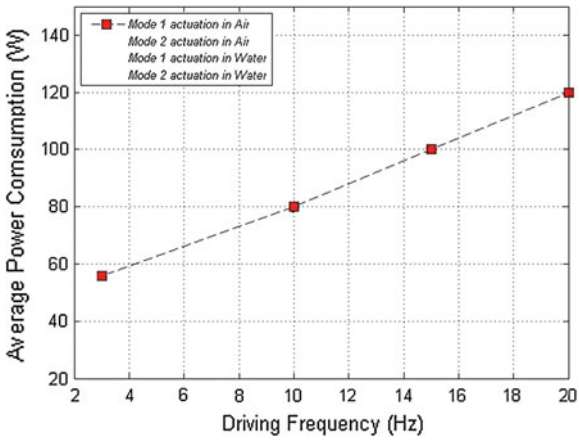

Fig. 18 Comparison of average electrical power consumption over driven frequency of both modes, actuating in air and water. No noticeable change was measured for both modes during actuation in air and in water

no noticeable increase in energy consumption was measured due to a resistance of the surrounding liquid. The result of high energy consumption can be significantly improved as the tests indicated large mechanical gains when actuating the mechanical drive system without link IV, reducing from a 120 to 70 W consumption. This was a result of pressure increase at higher velocities, as link IV was actuated; the tendons were required to be tighter to provide the desired posterior kinematics, putting increased strain on the mechanism. Despite the high energy consumption, the prototype can maintain an operational time of approximately 10 min at maximum velocity (estimated by video recording multiple runs), far surpassing the endurance of live fish, as equivalent burst speeds can only be maintained for short times of around one second. We can assume that engineering a greater mechanically efficient drive of link IV in the next generation may greatly improve endurance, relating to an estimated reduced energy consumption of approximately 50 %.

As illustrated in Fig. 19, the developed high power density ratio build can generate an incredible amount of force of up to 9 N. This can be effectively transferred in the water, accelerating both Modes to maximum velocity in approximately 0.6 s. The relationship between velocity (speed divided by body length) and driven frequency is shown in Fig. 20. The corresponding values of Modes 1 and 2 during consistent swimming are shown and compared to current robotic fish. Both operational Modes can achieve an average maximum velocity of 11.6 Bl/s, (i.e., 3.7 m/s) at 20 Hz, increasing performance in comparison with *iSplash*-I and current published robotic fish which typically peak around 1 BL/s. This result also outperforms the average maximum velocity of real fish measured at 10 BL/s. The values illustrated in Fig. 20 shows that applying the operational Mode 2 swimming pattern had no effect on performance due to kinematic alignment errors, discussed in Section IV–B, therefore it is predicted that the magnitude of added mass in both modes is equal. Hence, we can estimate that accurately applying

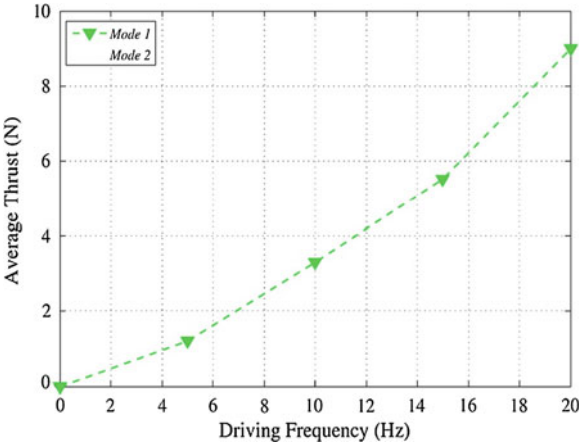

Fig. 19 Comparison of average thrust in relationship to driven frequency. Modes 1 and 2 have equivalent measurements

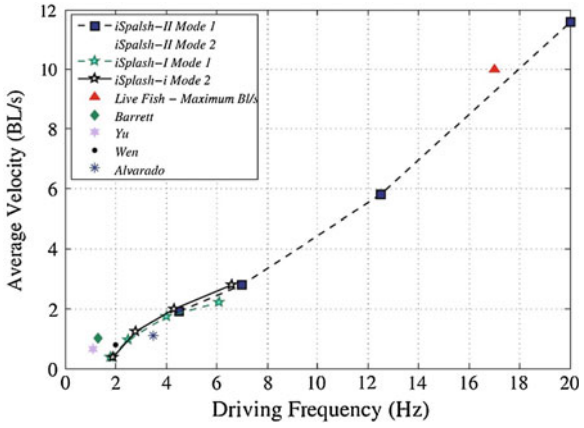

Fig. 20 Comparison of average velocities achieved by both modes, against robotic and live fish. Modes 1 and 2 measured equal velocities

the coordinated full-body swimming pattern of *iSplash*-I may increase speed by a further 27 %.

A prominent parameter for analyzing BCF locomotive performance is the Strouhal number (St), defined as $St = fA/U$, *w*here f denotes the frequency, A denotes the tail amplitude, and U is the average forward velocity. St is considered optimal within the range of $0.25 < St < 0.40$ [13]. The measured $St = 0.34$ under the condition of $Re = 1.2 \times 10^6$, in both Modes is within the desired range. The prototypes Swimming number (Sw) is highly efficient, measuring a Sw of 0.58 in comparison to the previous build with a Sw of 0.42 and close to the particular efficient common carp with a Sw of 0.70 [3, 10].

For this research we undertook experiments to gain knowledge if raising driven frequencies greater than the previous build of 6.6 Hz would continue to increase

speed without peak or decline. This was achieved measuring a continued increase in velocity up to intensively high frequencies of 20 Hz. Mimicking the swimming properties of real fish, frequency has become the key variable to enhance the linear locomotive performance of the *iSplash* platforms.

4 Conclusion and Future Work

This paper describes the development and experimental analysis of *iSplash*-I and *iSplash*-II. The experimental results of the first generation show conclusively that by coordinating the full-body length of the carangiform swimming motion a 27 % increase in performance, in terms of linear swimming speed, is gained over the traditional posterior confined wave form. The introduced full-body swimming motion can coordinate anterior, mid-body, and posterior displacements, and is able to reduce the kinematic errors seen in existing free swimming robotic fish. *iSplash*-I achieved a maximum velocity of 3.4 BL/s and consistently achieved a velocity of 2.8 BL/s at 6.6 Hz with a low energy consumption of 7.68 W.

A few points can be made to account for the increase in speed: The magnitude of propulsive force was increased by initiating the starting moment of added mass upstream; the developed structural arrangement allowed for smooth transition of flow along the length of body; anterior and/or mid-body vortices were formed, coordinated, and propagated downstream; lateral and thrust forces were optimized around the center of mass; a reduction in drag resistance due to reduced anterior amplitude errors. These points can be clarified in future experimental analysis utilizing visualization techniques which accurately measure the surrounding fluid flow. During the field trials the first generation prototype was found to increase its velocity as increased frequencies were applied in either swimming pattern, which indicated, that higher swimming speeds may be gained by raising frequency further.

The second generation was developed to realize the fastest speeds of live fish. A high-performance prototype was developed, robust, compact, naturally buoyant, carrying its own power supply, with a high power density and able to effectively transmit large forces at intensively high tail oscillation frequencies for untethered high-speed propulsion. Although the desired kinematics over the full-body could not be attained due to the power density requirements (with the primary actuator 75 % of the total mass), the devised assembly was able to reduce the recoil around the center of mass, therefore generating an effective propulsive mechanism. As a result, large posterior forces and tail amplitudes 0.2 of the body length (with smooth generated undulations from mid-body to tail tip) were attained. The prototype was able to accelerate to steady state swimming in an approximate time of 0.6 s, maintain an endurance at maximum speed for approximately 10 min (greater than the measurement of real fish of approximately one second), realize a highly efficient stride rate (Sw), and attain high tail oscillatory frequencies without early peak, decline, or mechanical failure.

iSplash-II, a 32 cm untethered carangiform swimmer, 0.835 kg, formed in PLA filament, consistently achieved a maximum velocity of 11.6 BL/s (i.e., 3.7 m/s) at 20 Hz with a stride rate of 0.58 and a force production of 9 N. The prototype is capable of outperforming the recorded average maximum velocity of real fish measured in BL/s, attaining speeds adequate for real world environments.

Future Work Our future research will focus on the following aspects: (i) continue to raise driven frequency to achieve greater speeds over the fastest real fish. As the build showed no signs of failure an initial aim of 40 Hz can be made; (ii) to accurately emulate the kinematic parameters of the full-body swimming motion of the first generation, indicating that maximum velocity may increase a further 27 %; (iii) to replace the drive mechanism of link IV, to significantly improve the energy consumption; (iv) to optimize the tail amplitude, shape, 3D deformation, and magnitude; (v) to apply the behavioral technique of burst and coast, as live fish generating 10 BL/s at the burst stage reduce the cost of transport by approximately 50 % [18]; (vi) to develop mobility within the horizontal plane with estimated turning diameter of <1 L

Acknowledgments Our thanks go to Richard Clapham senior for his technical assistance and financial contribution toward the project. This research was financially supported by a University of Essex Scholarship, as well as a research grant FI03005.

References

1. Bandyopadhyay PR (2002) Manoeuvring hydrodynamics of fish and small underwater vehicles. J Integr Comp Biol 42(1):102–117
2. Lighthill J (1975) Mathematical biofluiddynamics. Society for Industrial and Applied Mathematics, Philadelphia
3. Bainbridge R (1957) The speed of swimming of fish as related to size and to the frequency and amplitude of the tail beat. J Exp Biol 35:109–133
4. Barrett DS, Triantafyllou MS, Yue DKP, Grosenbaugh MA, Wolfgang MJ (1999) Drag reduction in fish-like locomotion. J Fluid Mech 392:183–212
5. Anderson JM, Chhabra NK (2002) Maneuvering and stability performance of a robotic tuna. J Integr Comp Biol 42(5):1026–1031
6. Yu J, Tan M, Wang S, Chen E (2004) Development of a biomimetic robotic fish and its control algorithm. IEEE Trans Syst Man Cybern Part B Cybern 34(4):1798–1810
7. Liu J, Hu H (2010) Biological inspiration: from carangiform fish to multi-joint robotic fish. J Bionic Eng 7:35–48
8. Wen L, Wu GH, Liang JH, Li JL (2010) Hydrodynamic experimental investigation on efficient swimming of robotic fish using self-propelled method. Int J Offshore Polar Eng 20:167–174
9. Valdivia P, Alvarado Y, Youcef-Toumi K (2003) Modeling and design methodology for an efficient underwater propulsion system. In: Proceedings IASTED international conference on robotics and applications, Salzburg
10. Nagai M (1999) Thinking fluid dynamics with dolphins. Ohmsha, LTD, Japan
11. Webb PW (1984) Form and function in fish swimming. Sci Am 251:58–68
12. Rosen MW (1959) Water flow about a swimming fish, China Lake, US Naval Ordnance Test Station TP 2298, p 96

13. Wolfgang MJ, Anderson JM, Grosenbaugh MA, Yue DK, Triantafyllou MS (1999) Near-body flow dynamics in swimming fish. J Exp Biol 202:2303–2327
14. Lauder GV, Drucker EG (2004) Morphology and experimental hydrodynamics of fish control surfaces. IEEE J Ocean Eng 29:556–571
15. Triantafyllou GS, Triantafyllou MS, Grosenbaugh MA (1993) Optimal thrust development in oscillating foils with application to fish propulsion. J Fluids Struct 7:205–224
16. Videler JJ (1993) Fish swimming. Chapman and Hall, London
17. Clapham RJ, Hu H, (2014) *iSplash*-I: high performance swimming motion of a carangiform robotic fish with full-body coordination. In: Proceedings of IEEE international conference on robotics and automation, Hong Kong
18. Videler JJ, Weihs D (1982) Energetic advantages of burst-and-coast swimming of fish at high speeds. J Exp Biol 97:169–178